Investigation of two-particle contributions to nucleon matrix elements

Constantia Alexandrou,[a,b] **Giannis Koutsou,**[b] **Yan Li,**[a,*] **Marcus Petschlies**[c] **and Ferenc Pittler**[b]

[a]*Department of Physics, University of Cyprus, P.O. Box 20537, 1678 Nicosia, Cyprus*

[b]*Computation-based Science and Technology Research Center, The Cyprus Institute, 20 Kavafi Str., Nicosia 2121, Cyprus*

[c]*HISKP (Theory), Rheinische Friedrich-Wilhelms-Universität Bonn, Nußallee 14-16, 53115 Bonn, Germany*

E-mail: li.yan@ucy.ac.cy

We investigate contributions of excited states to nucleon matrix elements by studying the two- and three-point functions using nucleon and pion-nucleon interpolating fields. This study is carried out using twisted mass fermion ensembles with pion masses 346 MeV and 131 MeV. We compare the results obtained using these two ensembles and show preliminary results for nucleon charges.

*Speaker

1. Introduction

Nucleon matrix elements $\langle N|J|N \rangle$ are important quantities to understand the structure of the nucleon. They can be extracted from the ratio of three- to two-point functions in the asymptotic limit:

$$\frac{\langle 0|O_N(t_{\text{sink}})J(t_{\text{ins}})\bar{O}_N(0)|0\rangle}{\langle 0|O_N(t_{\text{sink}})\bar{O}_N(0)|0\rangle} \xrightarrow{t_{\text{ins}}, \, t_{\text{sink}} \to \infty} \langle N|J|N\rangle \ . \tag{1}$$

The time separations used in practice, however, are limited and the ratio shows clear time dependence even at the largest available time separations. Since the time dependence comes from contributions of excited states, and the lowest excited state with the quantum numbers of the nucleon is a nucleon-pion state, we investigate the contribution of nucleon-pion states to the matrix elements.

2. Generalized eigenvalue problem (GEVP) and its impact on three-point functions

For a set of interpolating operators $\{O_i\}$ with fixed quantum numbers, one can compute the following matrix function:

$$C_{ij}(t) = \langle 0|O_i(t)O_j^\dagger(0)|0\rangle \ . \tag{2}$$

The generalized eigenvalue problem (GEVP)

$$C_{ij}(t)\, v_j^n = \lambda^n(t,t_0)\, C_{ij}(t_0)\, v_j^n \tag{3}$$

can determine the eigenvalue $\lambda^n(t,t_0)$ and eigenvector v_j^n of the n-th eigenmode. The eigenvectors should be independent of the reference time t_0. Solving the GEVP one extracts excited state energies E_n from eigenvalues $\lambda^n(t,t_0)$ via

$$\lambda^n(t,t_0) = e^{-E_n(t-t_0)} + \text{contributions from higher states.} \tag{4}$$

The GEVP also provides improved operators O_n' that increase the overlap with the n-th eigenstate by finding the optimal linear combination

$$O_n'\,|0\rangle \equiv v_j^n O_j^\dagger\,|0\rangle \propto |n\rangle \ . \tag{5}$$

Therefore, one can use the GEVP to construct an improved nucleon operator O_N' to obtain a ratio of three- to two-point functions with reduced time dependence:

$$\frac{\langle 0|O_N J\bar{O}_N|0\rangle}{\langle 0|O_N \bar{O}_N|0\rangle} \xrightarrow{\text{GEVP improved}} \frac{\langle 0|O_N' J\bar{O}_N'|0\rangle}{\langle 0|O_N' \bar{O}_N'|0\rangle} \ . \tag{6}$$

Here we consider a two-state model with $|N\rangle$ and $|N\pi\rangle$ to demonstrate how the GEVP works for three-point functions. We start with two interpolating operators O_N and $O_{N\pi}$. When acting on the vacuum they create states

$$\begin{aligned}
\bar{O}_N\,|0\rangle &= |N\rangle + x\,|N\pi\rangle + \cdots, \\
\bar{O}_{N\pi}\,|0\rangle &= |N\pi\rangle + y\,|N\rangle + \cdots,
\end{aligned} \tag{7}$$

Table 1: Decomposition of the improved three-point function $I = \langle 0|O'_N J \bar{O}'_N|0\rangle$. Each contribution should be multiplied with the corresponding matrix element in the first row and the time-dependent exponential terms.

	$\langle N|J|N\rangle$	$\langle N|J|N\pi\rangle$	$\langle N\pi|J|N\rangle$	$\langle N\pi|J|N\pi\rangle$
$I_1 = \langle 0|O_N J \bar{O}_N|0\rangle$	1	x	x	x^2
$I_2 = -x\, \langle 0|O_N J \bar{O}_{N\pi}|0\rangle$	$-xy$	$-x$	$-x^2 y$	$-x^2$
$I_3 = -x\, \langle 0|O_{N\pi} J \bar{O}_N|0\rangle$	$-xy$	$-x^2 y$	$-x$	$-x^2$
$I_4 = x^2\, \langle 0|O_{N\pi} J \bar{O}_{N\pi}|0\rangle$	$x^2 y^2$	$x^2 y$	$x^2 y$	x^2
$I = I_1 + I_2 + I_3 + I_4$	$(1-xy)^2$	0	0	0
$I' = I_1 + I_2 + I_3$	$1-2xy$	$-x^2 y$	$-x^2 y$	$-x^2$

where without loss of generality we take one of the coefficients to by unity, and we also suppress the time-evolution factors to simplify the notations and the ellipsis denote higher excited states. Then the improved nucleon operator O'_N satisfies

$$\bar{O}'_N |0\rangle \equiv (\bar{O}_N - x\, \bar{O}_{N\pi}) |0\rangle = (1 - xy) |N\rangle \, , \tag{8}$$

and the improved three-point function I can be expanded as

$$
\begin{aligned}
I &\equiv \langle 0|O'_N J \bar{O}'_N|0\rangle = \langle 0|(O_N - x\, O_{N\pi}) J (\bar{O}_N - x\, \bar{O}_{N\pi})|0\rangle \\
&= \langle 0|O_N J \bar{O}_N|0\rangle - x\, \langle 0|O_N J \bar{O}_{N\pi}|0\rangle - x\, \langle 0|O_{N\pi} J \bar{O}_N|0\rangle + x^2\, \langle 0|O_{N\pi} J \bar{O}_{N\pi}|0\rangle \, .
\end{aligned} \tag{9}
$$

Since the unimproved operators can both create two states as in Eq. (7), one can expand their three-point functions as follows

$$
\begin{aligned}
\langle 0|O_N J \bar{O}_N|0\rangle &= \langle N|J|N\rangle + x \langle N|J|N\pi\rangle + x \langle N\pi|J|N\rangle + x^2 \langle N\pi|J|N\pi\rangle \\
\langle 0|O_N J \bar{O}_{N\pi}|0\rangle &= y \langle N|J|N\rangle + \langle N|J|N\pi\rangle + xy \langle N\pi|J|N\rangle + x \langle N\pi|J|N\pi\rangle \\
\langle 0|O_{N\pi} J \bar{O}_N|0\rangle &= y \langle N|J|N\rangle + xy \langle N|J|N\pi\rangle + \langle N\pi|J|N\rangle + x \langle N\pi|J|N\pi\rangle \\
\langle 0|O_{N\pi} J \bar{O}_{N\pi}|0\rangle &= y^2 \langle N|J|N\rangle + y \langle N|J|N\pi\rangle + y \langle N\pi|J|N\rangle + \langle N\pi|J|N\pi\rangle \, .
\end{aligned} \tag{10}
$$

Therefore, one has 16 terms contributing to the improved three-point function as summarized in Table 1. In Table 1, elements from different columns should be multiplied with the matrix elements in the first row and the corresponding time-evolution factors, so for instance given our 2-state model

$$
\begin{aligned}
I_3 &= -x\, \langle 0\,|\,O_{N\pi}\, J\, \bar{O}_N\,|\,0\rangle \\
&= (-xy) \langle N|J|N\rangle\, e^{-E_N t_{\text{sink}}} \quad + \quad (-x^2 y) \langle N|J|N\pi\rangle\, e^{-E_N (t_{\text{sink}} - t_{\text{ins}}) - E_{N\pi} t_{\text{ins}}} \\
&\quad + (-x) \langle N\pi|J|N\rangle\, e^{-E_{N\pi} (t_{\text{sink}} - t_{\text{ins}}) - E_N t_{\text{ins}}} \quad + \quad (x^2) \langle N\pi|J|N\pi\rangle\, e^{-E_{N\pi} t_{\text{sink}}}
\end{aligned} \tag{11}
$$

Thus elements from different columns in Table 1 cannot be compared directly. Elements from different rows, however, can be summed up as already done in the table. The sum of the 4

Table 2: Parameters of the ensemble used in this work. Further details are given in Refs. [1–3]. The right-most column gives the number of gauge configurations employed N_{cfg}.

Ensembles	Flavors	$N_L^3 \times N_T$	a (fm)	m_π (MeV)	L (fm)	$m_\pi L$	N_{cfg}
cA211.53.24	2+1+1	$24^3 \times 48$	0.0947	346	2.27	3.99	2467
cA2.09.48	2	$48^3 \times 96$	0.0938	131	4.50	2.98	629

coefficients below each matrix element in the first row then gives the total contribution of this matrix element to the improved three-point function $I = \langle 0|O'_N\, J\, \bar{O}'_N|0\rangle$ in the 2-state model. Of course, the improved three-point function I receives zero contributions from matrix elements with $|N\pi\rangle$ states, which is borne out by the last-but-one row of the table.

Since I_4 is more difficult to compute, one can also look at the case $I' = I_1 + I_2 + I_3$. In this case, compared with the unimproved three-point function I_1, the contribution from $\langle N|J|N\pi\rangle$ or $\langle N\pi|J|N\rangle$ changes from x to $-x^2 y$, and the one from $\langle N\pi|J|N\pi\rangle$ changes from x^2 to $-x^2$. If the contamination from the former is large, one should observe a significant change from I_1 to I' as long as $-xy$ is not close to 1. Considering that $-xy \approx 1$ would indicate $O_N|0\rangle = |N\rangle + x|N\pi\rangle$ and $O_{N\pi}|0\rangle \approx y(|N\rangle - x|N\pi\rangle)$ share a similar composition, it is unlikely to happen. If the contamination from the latter is large, one should also observe a significant change because the sign of the contamination would flip. Therefore, one should see a significant change if any of these $N\pi$ contamination terms are large. Contrary, if no change is observed, one can conclude that the contamination does not come from the $N\pi$ state under consideration.

3. Lattice setup

We use two ensembles, one with a physical pion mass, the other one with a heavier pion mass, simulated using twisted mass clover-improved fermions as indicated in Table 2.

We consider single nucleon and nucleon-pion operators at various momenta. We compute both the two- and three-point functions between them. For the three-point functions, $\langle 0|O_{N\pi} J \bar{O}_N|0\rangle$ can be obtained via symmetry from $\langle 0|O_N J \bar{O}_{N\pi}|0\rangle$, and $\langle 0|O_{N\pi} J \bar{O}_{N\pi}|0\rangle$ has not been included in this work. All the diagrams considered are summarized in Fig. 1. Diagrams with pion loops are also included, because they are non-zero in twisted-mass lattice QCD, which breaks isospin symmetry. The three diagrams involving an insertion loop are still under investigation, and will not be included here.

Diagrams without loops were carried out in a similar way as in Ref. [4]. For loops, we compute them stochastically with time dilution.

4. Lattice results

In Fig. 2, we show the results for the effective energies and eigenvector components determined by the GEVP. The effective energies show stability and asymptotically they yield values that are consistent with the nucleon and πN non-interacting energies. The eigenvector components also show stability from around the same t_{sink} as those for the effective energies.
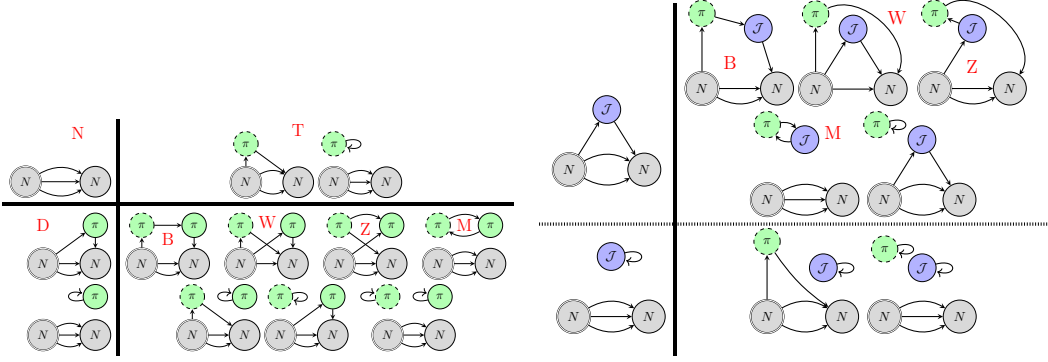
Figure 1: Different types of diagrams for two- (left) and three-point (right) functions under study.
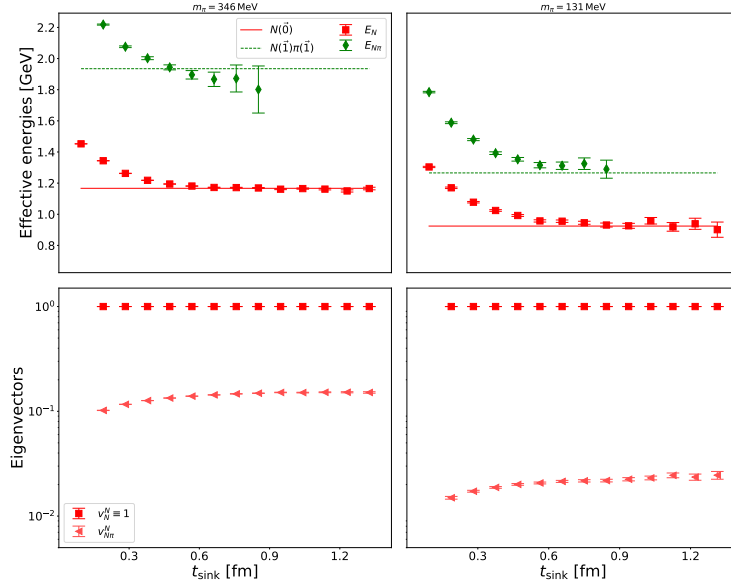

Figure 2: Effective energies and eigenvector components determined from the GEVP matrix of two-point functions. Horizontal lines in the effective energy plots are for the nucleon and the non-interacting $N\pi$ levels.

In Fig. 3, we show the results for the ratio of three- to two-point functions before and after the GEVP improvement. The upper panels are for zero transfer momentum $Q^2 = 0$. The first row is for the connected contribution to the πN-σ term charge g_S^{u+d}. In this case, there are no significant changes between improved and unimproved matrix elements for both ensembles. Based on the discussion of the previous section, we conclude that large excited state contamination in matrix element of the scalar operator from the lowest πN state is unlikely. For the axial charge g_A^{u-d}, shown in the panels in the second upper row, we also do not observe significant changes. However, in this case, unlike for the matrix element of the scalar operator, no strong time-dependence is observed even before improvement using the GEVP. We also examine several combinations varying the current insertion and the momentum transfer. While for most of them we observe no significant changes, for a few cases there is improvement as discussed below. We show results for

the pseudoscalar $\bar{G}_5(Q^2)$ and induced pseudoscalar $\bar{G}_p$ form factors with pion pole removed in the third, fourth and fifth rows of Fig. 3 for one lattice unit of momentum transfer, $Q^2 = 0.283$ GeV^2 and 0.074 GeV^2, for the CA211.53.24 and cA2.09.48 ensembles respectively. Each of these quantities shows a strong time dependence indicating high contribution from excited states. All of them show significant changes after applying the GEVP. Using the improved interpolating field, they show reduced time dependence, and in many cases, converge to a given constant around $t_{\text{ins}} = t_{\text{sink}}/2$. Most of the contamination is removed in particular for $\bar{G}_{p,t}(Q^2)$ computed using the axial vector in the temporal direction showing indeed that πN states are responsible for the contamination.

In those cases where a significant change is seen, there are five diagrams without an insertion loop for the $\langle 0|O_N J\bar{O}_{N\pi}|0\rangle$ as shown in Fig. 1. It turns out to be that the diagram labelled as 'M' makes the dominant contribution. This was also observed in Ref. [6]. It is also worthy noting that this diagram was observed to be enhanced only if the insertion operator can couple to the pion. This supports the chiral-perturbation-theory argument made by Refs. [7, 8].

5. Conclusions

We use an improved nucleon interpolating field constructed from the GEVP to compute the three- to two-point function ratios for various nucleon form factors. We find that excited state contamination in the scalar and axial charges matrix elements is unlikely to come from the lowest πN state, while for the pseudoscalar and induced pseudoscalar form factors a significant improvement is observed.

ACKNOWLEDGEMENTS

References

[1] ETM collaboration, *First Physics Results at the Physical Pion Mass from $N_f = 2$ Wilson Twisted Mass Fermions at Maximal Twist*, *Phys. Rev. D* **95** (2017) 094515 [1507.05068].
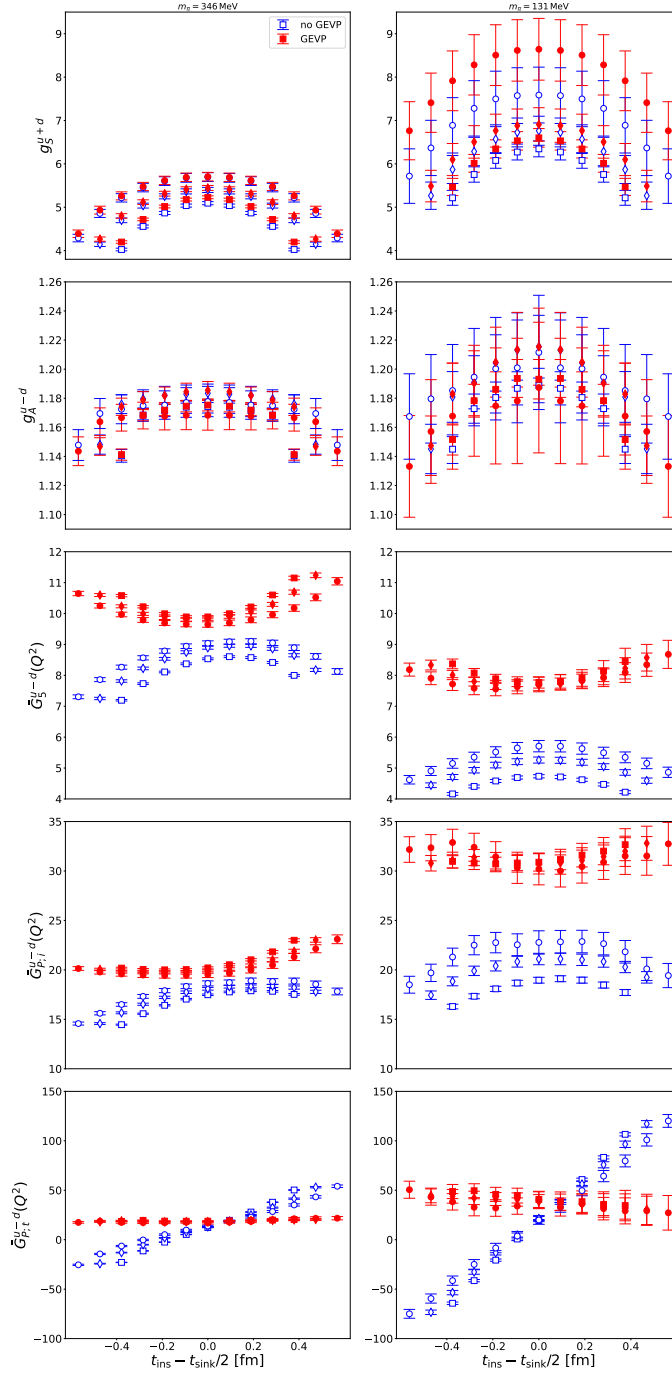
Figure 3: Ratios of three- to two-point functions before and after the GEVP improvement. Results are shown for $t_{\text{sink}} = 10a$ (square), $12a$ (diamond), $14a$ (circle) with different shapes. From top to bottom, the ratios are for the (connected) scalar charge g_S^{u+d}, axial charge g_A^{u-d}, modified pseudoscalar form factor $\bar{G}_5^{u-d}(Q^2)$, and modified induced pseudoscalar form factors $\bar{G}_{P;i}^{u-d}(Q^2)$ and $\bar{G}_{P;t}^{u-d}(Q^2)$, where Q^2 corresponds to one lattice unit of momentum, $G_{P;i}$ and $G_{P;t}$ are extracted from the spacial and temporal axial matrix elements, respectively, and the modified form factors are related to the form factors via $\bar{G}_5 = \frac{m_\pi^2 + Q^2}{F_\pi m_\pi^2} m_q G_5$ and $\bar{G}_P = \frac{m_\pi^2 + Q^2}{F_\pi m_\pi^2} \frac{Q^2}{4m_N} G_P$. We adopt the same conventions for these form factors as in Ref. [5].

[2] C. Alexandrou, S. Bacchio, P. Charalambous, P. Dimopoulos, J. Finkenrath, R. Frezzotti et al., *Simulating twisted mass fermions at physical light, strange and charm quark masses*, *Phys. Rev. D* **98** (2018) 054518 [`1807.00495`].

[3] EXTENDED TWISTED MASS collaboration, *Quark masses using twisted mass fermion gauge ensembles*, *Phys. Rev. D* **104** (2021) 074515 [`2104.13408`].

[4] C. Alexandrou, S. Bacchio, G. Koutsou, T. Leontiou, S. Paul, M. Petschlies et al., *Elastic Nucleon-Pion scattering amplitudes in the Δ channel at physical pion mass from Lattice QCD*, *arXiv:2307.12846 [hep-lat]* (2023) [`2307.12846`].

[5] C. Alexandrou, S. Bacchio, M. Constantinou, J. Finkenrath, R. Frezzotti, B. Kostrzewa et al., *Nucleon axial and pseudoscalar form factors using twisted-mass fermion ensembles at the physical point*, *arXiv:2309.05774 [hep-lat]* (2023) [`2309.05774`].

[6] L. Barca, G. Bali and S. Collins, *Towards N to $N\pi$ matrix elements from Lattice QCD*, *Phys. Rev. D* **107** (2023) L051505 [`2211.12278`].

[7] O. Bar, *$N\pi$-state contamination in lattice calculations of the nucleon axial form factors*, *Phys. Rev. D* **99** (2019) 054506 [`1812.09191`].

[8] O. Bar, *$N\pi$-state contamination in lattice calculations of the nucleon pseudoscalar form factor*, *Phys. Rev. D* **100** (2019) 054507 [`1906.03652`].

PoS(LATTICE2023)080